A98-31636

ICAS-98-5,4,3

ON THE STEADY AND UNSTEADY EFFECTS OF BLADE ROW SPACING IN A COUNTERROTATING DUCTED PROPFAN

Lothar Wallscheid
German Aerospace Center
Institute of Propulsion Technology
Cologne, Germany
EMail: lothar.wallscheid@dlr.de

Abstract

Steady and time-accurate unsteady 2D viscous calculations have been carried out on a cylindrical slice of a transonic counterrotating ducted propfan to study the effects of blade row spacing on the steady and unsteady flow behavior. Therefore three different spacings between the two rotors have been simulated. The steady results show deviations for the individual cases, probably due to various error sources in the approach. The results show that there is a strong dependency of the distance on the unsteady flow. Especially between the rotors the upstream potential effects of the second rotor are apparent. Behind the rotors the amplitudes are smaller but still dependent on the blade row spacing. The amplitude of the unsteady contributions is dependent upon the circumferential position in the blade passage. The envelopes of the unsteady variables are similar between the rotors regardless of the axial spacing. However, downstream of rotor 2 the shape of the envelopes varies with the blade row spacing.

Nomenclature

Variables

α	Angle, °
α	Circumferential angle, absolute system, °
β	Circumferential angle, relative system, °
c	Absolute velocity, m/s
d	Geometric distance, m
f	Frequency, $1/s$, Hz
γ	Radial angle, °
h	Streamtube thickness, m
l	Chord length, m
Ma	Mach number
m	Number
n	Rotational speed, m/s
n	Number
p	Pressure, Pa
π	Pressure ratio
R	Gas constant, $J/(kgK)$
r	Radius, m
t	Time, s
u	Circumferential velocity, m/s
w	Relative velocity, m/s
ω	Angular velocity, $1/s$
x	Axial Distance, Coordinate, m
y	Coordinate, m
z	Coordinate, m

Indices

∞	refers to ambient state
1	refers to rotor 1
2	refers to rotor 2
abs	refers to absolute frame of reference
e	exit value
i	inlet value
r	radial component
rel	refers to relative frame of reference
s	static value
t	total value
u	circumferential component
x	axial component

Abbreviations

b.c.	boundary conditions

Introduction

Future jet engines will have higher bypass ratios than today to achieve a better propulsion efficiency. One alternative of the various proposed engine types is the CRISP* engine, which has been introduced by MTU, Germany. It consists of two transonic counterrotating rotors designed for axial in- and outflow. A 1m-diameter model of this

*. CRISP: CounterRotating Integrated Shrouded Propfan

engine is investigated experimentally and numerically at DLR, Cologne, with respect to aeroacoustic, aerodynamic and aeroelastic viewpoints.

Measurements of the unsteady absolute total pressure ratio over both rotors show large fluctuations up to 30 % of the overall total pressure rise at the measured radius[5]. This is one good reason to look into the details of the unsteady flow phenomena inside the blade rows. Therefore measurements of the unsteady velocity vector (with a 3D-L2F-System) and unsteady absolute total pressure and simulations of the unsteady flow field have been carried out. To reduce the experimental and numerical effort the range of investigations have been reduced to a cylindrical slice at approximately 60 % blade height in a first step. This radius has been chosen with respect to the position where the second rotor faces the highest inlet relative Mach number. A second aspect for the selection of the radius is the absence of strong 3D-effects outside the wake regions in this part of the flowfield.

In [4] and [5] it is shown that there are mainly three unsteady phenomena affecting the energy transfer to the fluid. First, there is the interaction between the rotor 1-generated wakes and the profiles of rotor 2. Then, there is the reflection of the shockwave originating from rotor 2 on the pressure side of rotor 1 and third the interaction of the reflected shock wave with the profiles of rotor 2. These phenomena contribute to the local and time-limited circumferential flow turning in the flowfield of both rotors.

In this paper the impact of the distance of the two blade rows as the only parameter on the aforementioned phenomena and the energy transfer to the fluid is investigated. Therefore, 2D-simulations of the unsteady and viscous flow have been carried out for three different distances. A closer look is then taken at the time-mean values and the enevelopes on positions downstream of rotor 1 and downstream of rotor 2. The entry and exit conditions have been kept constant for all cases. One case is the original (designed case). This will be denominated case 'O' (original distance). For the second case the distance has been reduced by 20 % . This case will be referred to as case 'S' (shortened distance) while for the last case the distance has been increased by 20 % (case 'L' (lengthened distance)). Table 1 lists the selected parameters for the three

	Case 'S'	Case 'O'	Case 'L'
Chord length l_1, mm	163	163	163
Chord length l_2, mm	163.5	163.5	163.5
Axial distance d, mm	80	100	120
Axial distance, % l_1	49.08	61.35	73.62
Axial distance, % l_2	48.93	61.16	73.39

Table 1: Variation of axial distance in absolute values and related to chord length

Parameter	Value
Entry absolute total pressure $p_{t,abs,1,i}$	101325 Pa
Entry absolute total temperature $T_{t,abs,1,i}$	288.15 K
Entry absolute circumferential angle $\alpha_{1,i}$	0°
Exit static pressure ($p_{s,e}/p_{t,i}$)	0.9753
Streamtube thickness h	see text
Circumferential velocity rotor 1 u_1	184.1 m/s
Circumferential velocity rotor 2 u_2	159.6 m/s

Table 2: Boundary Conditions for 2D-simulation

kinematic boundary conditions for the investigated case. A closer look at the variation of the streamtube thickness in axial direction will be made in section 'Approach'.

CRISP-configuration

As mentioned in the section before the investigated compressor is a counterrotating fan stage designed for UHB-engines. The absolute axial inlet Mach number $M_{abs,i}$ is high (approx. 0.77) and the overall absolute total pressure $\pi_{t,abs}$ ratio is quite low (approx. 1.3). Fig. 1 shows some

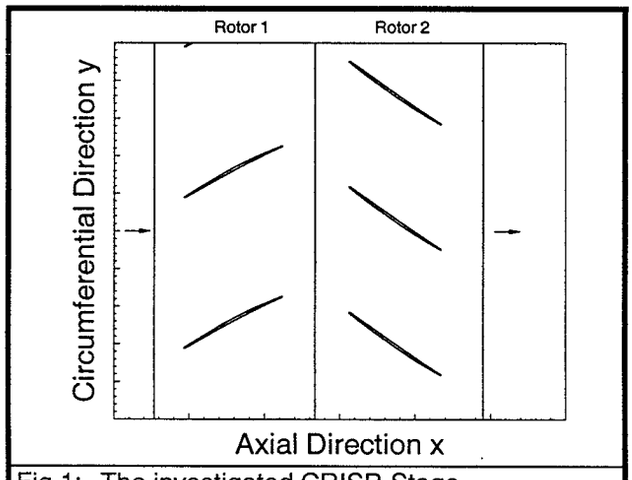

Fig.1: The investigated CRISP-Stage

passages on the selected slice for both rotors. The airflow is from left to right as indicated by the arrows. Rotor 1 moves downwards and rotor 2 advances in upward direction. The blade number of rotor 1 is 10, rotor2 consists of 12 blades. Therefore, the blade count ratio of the rotors is 5/6. The pitch to chord ratio is approx. 1.36 for the first and 1.13 for the second rotor.

Approach

Boundary Conditions

As described in [4], the boundary conditions listed in Table 2 plus the axial distribution of the streamtube thickness for the 2D-slice have been derived from a steady 3D Navier-Stokes calculation. The code used for this calculation TRACE[3]. With these b.c.'s first a 2D steady Navier-

Stokes simulation is carried out. The steady solution is then used as initial guess for the unsteady simulation. The last two steps have been performed using the flow solver TRACE[2].

The prescription of the streamtube thickness variation is as follows (see Fig. 2): For any stage two axial with two

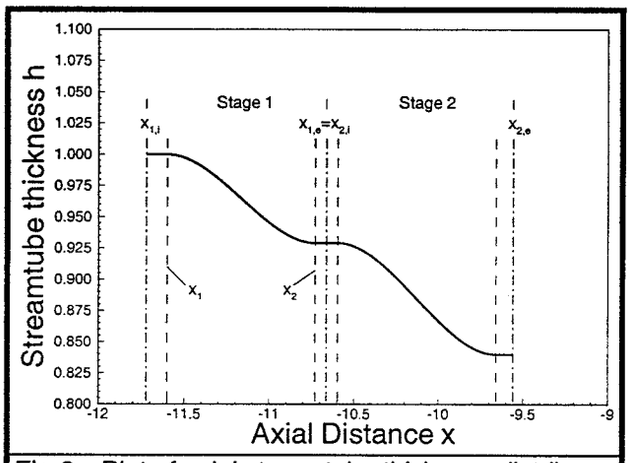

Fig.2: Plot of axial streamtube thickness distribution

thickness values are provided. Between the dash-dotted and the dotted line on the left side and the dashed and dash-dotted line on the right of stage 1 the thickness is kept constant. Between the dashed lines there is a symmetric and hyperbolic distribution. The connection between the constant and the hyperbolic part is smooth up to the first derivative with respect to the axial direction. The streamtube thickness variation is accounted for by an appropriate source term in the flow equations.

Parameter variation

The three cases for the parameter variation have been described in section 'Introduction'. The remaining parameter to be determined is the streamtube thickness distribution for the different axial spacings. The distribution is adapted in a way that the axial positions of the connections (x_1, x_2) between the constant and hyperbolic part does not change relative to the profile of the respective stage. The whole hyperbolic part moves according to the profile movement. Only the axial lengths of the constant parts changes. Since the code uses non-reflecting, far-field boundary conditions, this should not cause significant changes for the steady flow in a numerically ideal situation. In reality there will be a difference even in the steady case due to limited mesh resolution especially at the boundaries and in the wake regions. Due to different path length from the profiles to the exit boundaries the wake-mixing process will be erroneous and cause the operating point to be different. Fig. 3 shows the streamtube thickness distributions for the three cases.

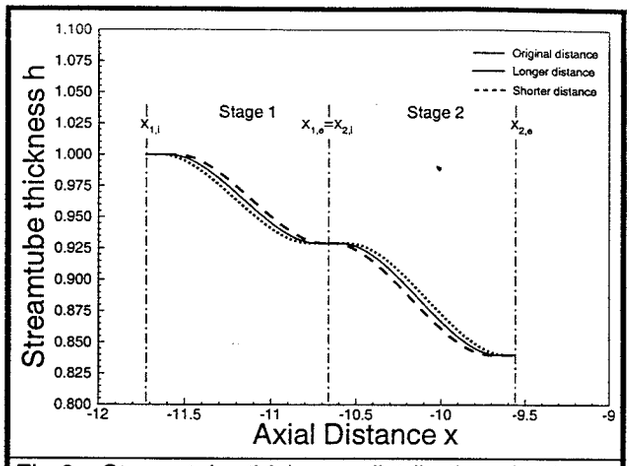

Fig.3: Streamtube thickness distributions for the three different cases

Calculation of envelopes and time mean values

The data analysis includes the time-mean values and envelopes of the time dependent flow. These values are calculated fixed to the respective rotor over one blade passing period. It is assumed that the flow pattern in a passage of the first rotor is periodic with each passage of the second rotor passing by the observer (fixed to rotor 1) and vice versa.

During this period the maximum and minimum value is searched and the time mean is calculated for the circumferential positions. The maximum values are then represented by the upper envelope curve and the minimum values by the lower envelope curve. It is stressed that the envelope curves do not represent one instantaneous flow picture but the extremum values at each circumferential position regardless of the time and number of their occurrence.

Results And Discussion

Overview

Fig. 4 is intended to introduce the overall steady flow behavior. For each stage two rotor passages are plotted. The different gray levels render the relative Mach number M_{rel}. The air enters the first rotor on the left. Around the leading edge there is a strong acceleration of the flow to transonic velocities. The peak value of the pre-shock Mach number is 1.27. The transonic area is terminated by a shock. The shock is almost perpendicular in the relative frame of reference. Behind the shock no further strong gradients with respect to relative Mach number can be found. The overall flow turning (absolute frame of reference) is approx. 17°. In the second stage a similar flow pattern can be noticed. There is also a strong expansion around the leading edge of the profile. The peak pre-shock Mach number is 1.4. The overall flow turning in the absolute frame of reference is 20°, leaving approx. 3° swirl

behind the second stage. The design point shows a swirl free flow at the exit of the second rotor. In this case the absolute total pressure ratio is higher, resulting in the aforementioned overturning.
The unsteady flow features are shown in Fig. 5. The different gray levels show the instantaneous distribution of the absolute value of the spatial density gradient. Again, the expansion areas and the shockwaves of both rotors can clearly be seen. Inside rotor 2 the transport of the rotor 1-generated wakes are reproduced. Furthermore, there is the interaction between the rotor 2-generated shockwaves and rotor 1. Note the strong bending of the shock when it enters the passage of the first rotor. This shock is reflected on the pressure side of the rotor 1 blades. The reflected wave moves almost circumferentially with a small downstream component. The wave then enters the rotor2 again, interacting with its blades. Another wave spreads from the pressure side of rotor 2 when the rotor 1-generated wakes hit the leading edge and pressure side of rotor 2.

Steady flow

For the steady flow the values α, M_{abs}, $p_{t,abs}$ will be compared in front of, between (two positions) and behind the rotors for all three cases. Fixed in position relative to their respective profiles two positions per rotor will be shown.
Fig. 6 shows circumferentially extracted values upstream and downstream of rotor 1. The axial position of the extraction lines is fixed relative to the profile coordinates. The left column contains the upstream and the right column the downstream values.
The upstream absolute Mach number shows little change in the expansion area, but the shock position varies slightly. With increasing distance the shock moves downstream. Due to the present shock angle the change in position in chord direction is smaller than in the circumferential direction (see Fig. 4). Basically the same is true for the α- and $\pi_{t,abs}$-distributions. A trend is visible from the smallest to the highest axial distance. Downstream of rotor 1 deviations of the α- and M_{abs}-values are visible for case 'L', but the absolute pressure ratio is equal. It seems that the operating point is slightly different for this case.
Upstream and downstream of rotor 2 (see Fig. 7) the deviations for the three cases grow larger, although the shock position inside the rotor 2-passage is somewhat more stable. The upstream values show no clear trend for the three different axial distances.
The reason for these deviation are likely to be found in the numerics and/or the used approach. However, it is difficult to 'blame' the code, approach or the choice of boundary conditions, since a boundary condition, reflecting or non-reflecting, far-field or non-far-field uses a certain method of averaging and this result is dependent on the distance between profile and boundary (e.g. the different wake profiles at the boundaries).

Unsteady flow

The comparison of the three cases with respect to the unsteady flow is made downstream of rotor 1 and rotor 2. For the three variables M_{abs}, α, $\pi_{t,abs}$ the envelope and the time-averaged values are calculated. When calculating the maximum differences between the minimum and maximum envelope curve the wake regions of the respective rotor are not considered.

Downstream Rotor 1

Fig. 8 shows the respective values for the position downstream of rotor 1. The left column contains the plots of the absolute Mach number M_{abs}, the middle column shows the α-angle and the right column covers the absolute total pressure ratio $\pi_{t,abs}$. The upper row represents case 'L', the middle row case 'O' and the lower row represents case 'S'. The values are plotted over 2 passages of rotor 1 (72 degrees). The dashed lines show the maximum values, the dotted lines show the minimum values and the solid lines display the time-mean values.
Beginning with the absolute Mach number, it can be seen that with decreasing distance the amplitude (i.e. the difference between maximum and minimum curve) increases. The amplitude is almost constant over the whole pitch, even in the wake area. The difference in absolute Mach number between minimum and maximum envelope is 0.1 for case 'L', 0.14 for case'O' and 0.2 for case 'S'. The time-mean values are growing with decreasing distance. The Mach number seems to be dominated by the potential upstream effects of rotor 2, since the amplitude is very stable and the distance between the rotors is of great effect.
Regarding the absolute circumferential angle α, it can be noticed that the difference between minimum and maximum envelope is rising with the distance becoming smaller. On the contrary to the absolute Mach number, the amplitude is not constant throughout the rotor 1 passage. There are three positions in one passage where the difference between minimum and maximum level is minimal. The basic shape of the envelope curves is similar for all three cases. The potential upstream effects of rotor 2 should have produced curves like these in the Mach number plots, so there must be other phenomena related to rotor 1 causing the deviations. One effect might be the reflections of the shockwave of rotor 2 on the pressure side of rotor 1 (see Fig. 5). The maximum amplitude of the α-Distribution is 5.2 degrees for case 'L', 7.6 degrees for case 'O' and 8.4 degrees for case 'S'. The shape of the time-mean curve is similar for all three cases. The flow turning in the absolute system seems to be somewhat smaller in case 'L'.
Similar can be observed for the absolute total pressure ratio downstream of rotor 1. The amplitude of the minimum and maximum envelope rises with decreasing distance. The difference between the two curves is not constant throughout the blade passage and again, the shape of the curves are similar for all three cases. The maximum

distance between the envelope curves is 76 *mbar* for case 'L', 96 *mbar* for case 'O' and 125 *mbar* for case 'S'. The time-mean curves become 'smoother' with decreasing distance, the time-mean of case 'L' being slightly higher than of the other two cases.

Downstream Rotor 2

The same view of the selected variables M_{abs}, α, $p_{t,abs}$ but now for the position downstream rotor 2 shows Fig. 9. Because of the absence of any additional upstream effects due to downstream blade rows the signal only consists of unsteady upstream phenomena.

The Mach number plots still show significant differences between the maximum and minimum envelope. The overall amplitude is almost equal for all three cases. The reason for the time mean value being close to the maximum envelope is as follows: The minimum envelope curve is formed by the wakes of rotor 1 as they are transported through rotor 2. As these wakes are only of small width, they do not contribute very much to the time-mean value. On the other hand it can be recognized by the shape of the minimum envelope, that the (rotor 1-) wake absolute Mach number deficit is not constant. Additionally, the shape of the minimum envelope varies with decreasing distance. The reason for this must be the different streamline length between the three cases causing unsteady interactions to take place at different timesteps. The same is true for the maximum envelope. The overall amplitudes (maximum difference case 'L': 0.052, case 'O': 0.046, case 'S': 0.06) show a slight increase with decreasing distance and the time-mean values are at the same level for all cases.

Similar observations can be made for the absolute circumferential angle α. The shape of the envelope curves varies in all cases due to the different development of the unsteady phenomena. The maximum differences between the minimum and maximum curve is 4 degrees (case 'L'), 3,6 degrees (case 'O') and 2,7 degrees (case 'S'), so there is a decrease in amplitude with decreasing distance. The shape and level of the time-mean values is equal for case 'O' and 'S'. The plot for case 'L' shows a different contour and is at a slightly lower level (approx 0.5 degrees difference).

For the absolute total pressure ratio again it can be said that the amplitude shows an increase with decreasing distance. The shapes of the envelope curves, especially the minimum envelope, vary as the case arises. The maximum difference between the envelopes is 85 *mbar* for case 'L', 89 *mbar* for case 'O' and 95 *mbar* for case 'S'. Related to the overall total pressure rise there is a total pressure fluctuation of approx. 27 %. The lower envelope is formed by the rotor 1-generated wakes. In contrast to the absolute Mach number the time-mean values are well between the minimum and maximum curve. Therefore it seems that the phenomena causing the higher absolute total pressure are of equal width and intensity. For case 'L' the level of the time-mean absolute total pressure is slightly lower than in the other to cases. This corresponds to the lower circumferential flow angle.

Conclusion and Outlook

A parameter variation with respect to the axial distance of two counterrotating transonic rotors has been carried out to analyze the intensity of the unsteady phenomena downstream of rotor 1 and 2. The results from the steady computations are dependent on the blade row spacing. The reason are mainly to be found in the numerical approach, e.g. the averaging in the boundaries or the streamtube thickness prescription. Therefore, no physical interpretations are deduced from the computed results.

The presented values α, M_{abs}, $p_{t,abs}$ downstream of rotor 1 show a strong dependency on the axial spacing between the two rotors. The main reason for this are the strong potential upstream effects of the transonic second rotor. Downstream of rotor 2 the dependency of these variables on the distance is smaller, but still visible. It is obvious, that the flow turning in the absolute system is an important parameter for the energy transfer to the fluid. It remains to be investigated if there is a criterion for the choice of the axial distance from the aerodynamical point of view. From the aeroacoustical and aeroelastical point of view this question is likely to be of greater importance. These investigations have yet to be carried out.

Acknowledgments

The author wishes to thank all people who have contributed to this work, especially Mr. F. Eulitz, who is in charge of developing the unsteady code TRACE. The project is funded by BMBF, project Engine3E, project number LFT 9601.

Literature

[1] Gallus, H.E.; Grollius, H.; Lambertz, J., 1982 "*The Influence Of Blade Number Ratio and Blade Row Spacing On Axial-Flow Compressor Stator Blade Dynamic Load And Stage Sound Pressure Level*", ASME-Paper 81-GT-165

[2] Eulitz, F.; Engel, K.; Gebing, H., 1996, "*Numerical Investigation Of The Clocking Effects in A Multistage Turbine*", ASME 96-GT-26

[3] Vogel, D.T., 1996, "*Numerische Untersuchung des Mischungsverhaltens von Filmkühlstrahlen in Turbinenströmungen*", DLR-FB 96-35

[4] Wallscheid, L; Eulitz, F., 1997, "*Investigation of Rotor/Rotor-Interaction*", XIII Isabe, Paper No. IS126/GE6

[5] Wallscheid, L.; Eulitz, F.; Heinecke, R., 1998, "*Investigation Of Unsteady Flow Phenomena in A Counterrotating Ducted Propfan*", to be presented at ASME Turbo Expo 98, 02.-05. June 1998, Stockholm, Sweden

Appendix

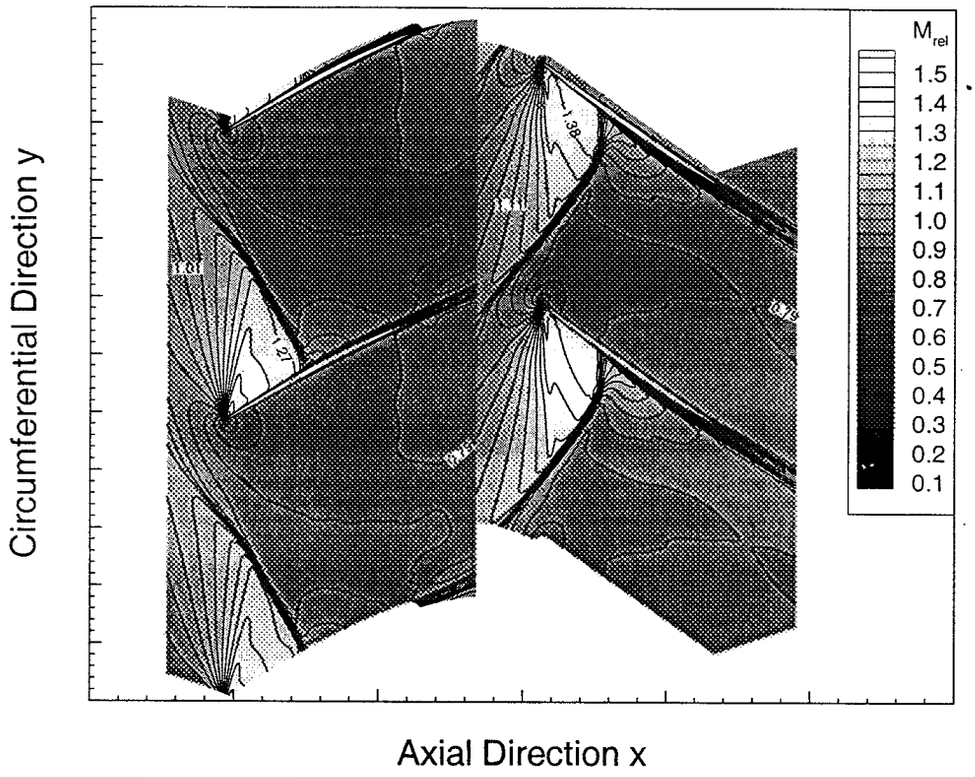

Fig.4: Relative Mach number M_{rel} for steady solution of case 'O'

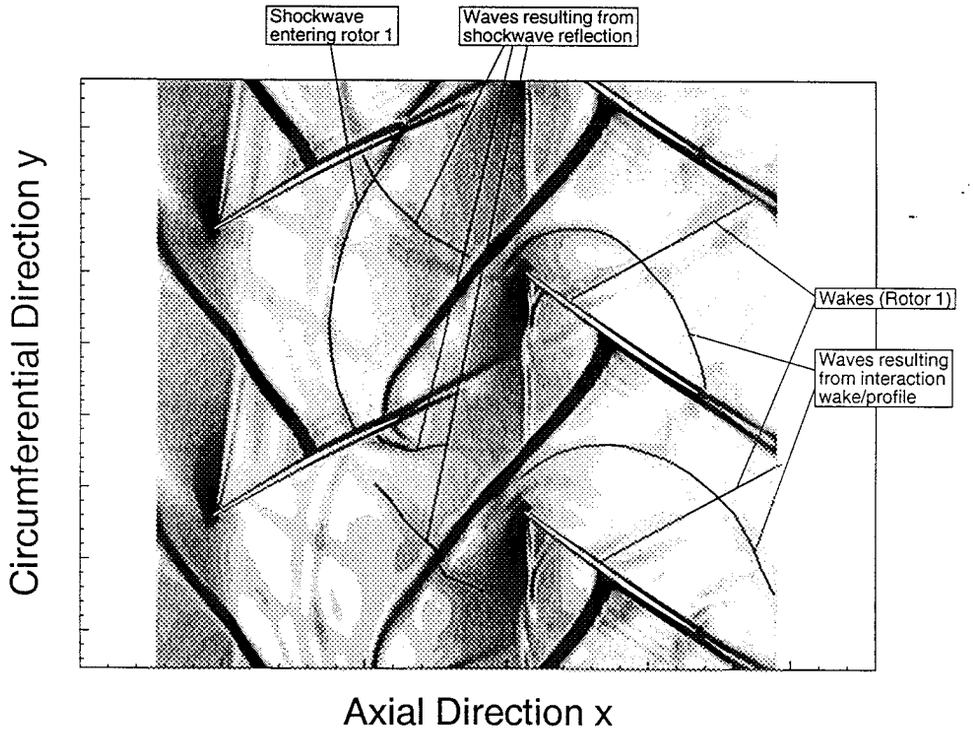

Fig.5: Instantaneous distribution of the unsteady spatial density gradient for case 'O'

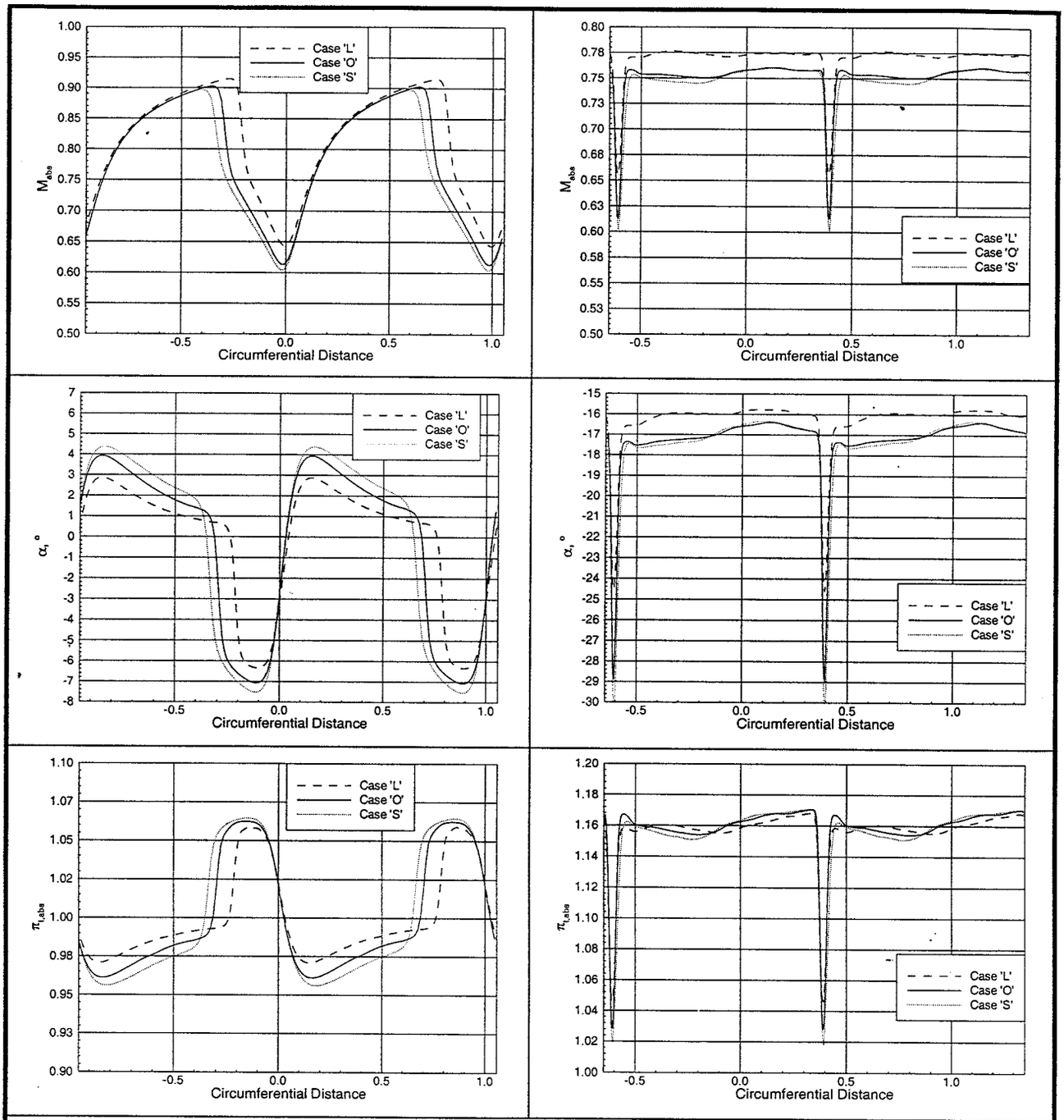

Fig.6: M_{abs}, α, $p_{t,abs}$ for steady flow upstream (left column) and downstream (right column) of rotor 1

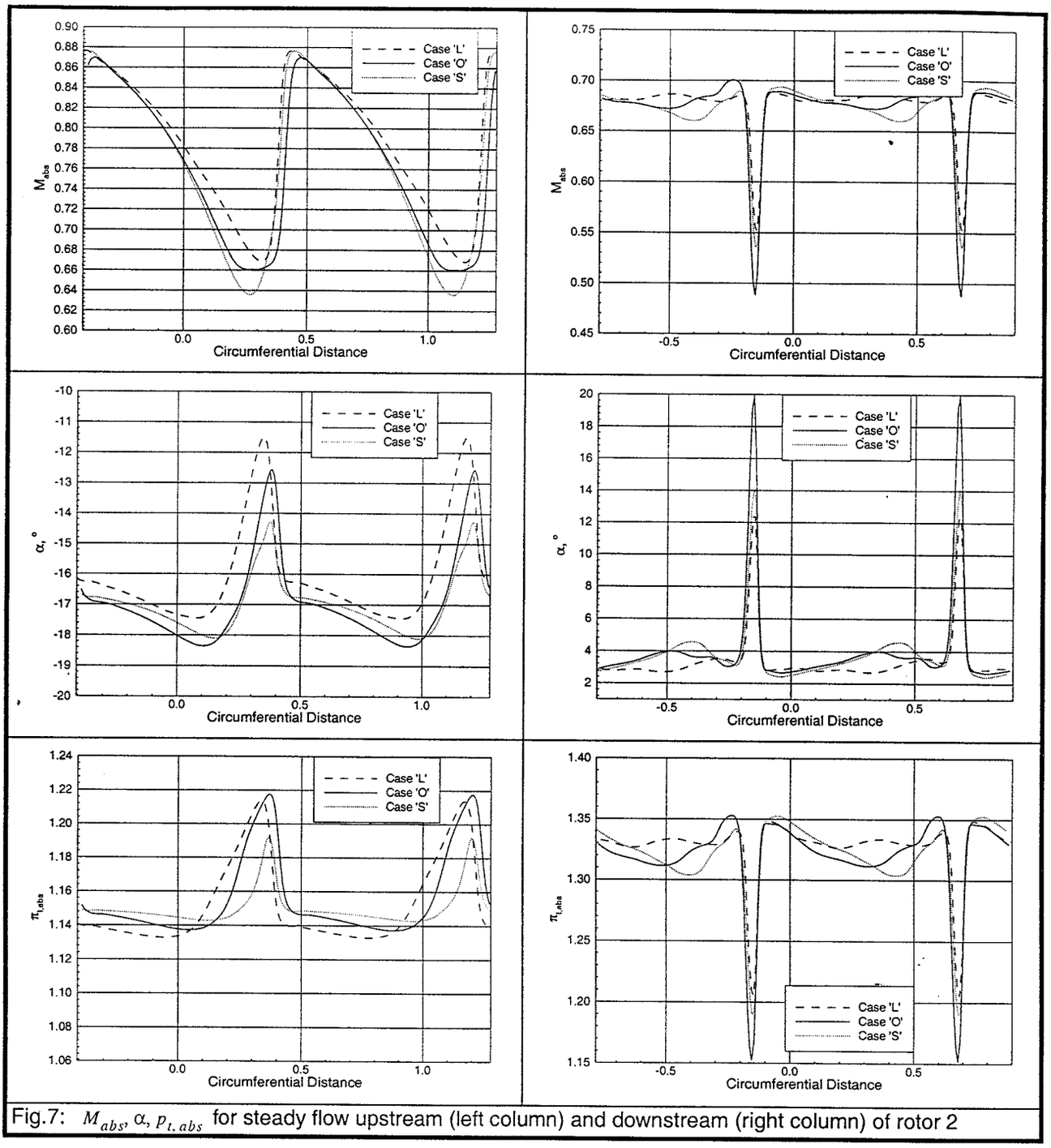

Fig.7: M_{abs}, α, $p_{t,abs}$ for steady flow upstream (left column) and downstream (right column) of rotor 2

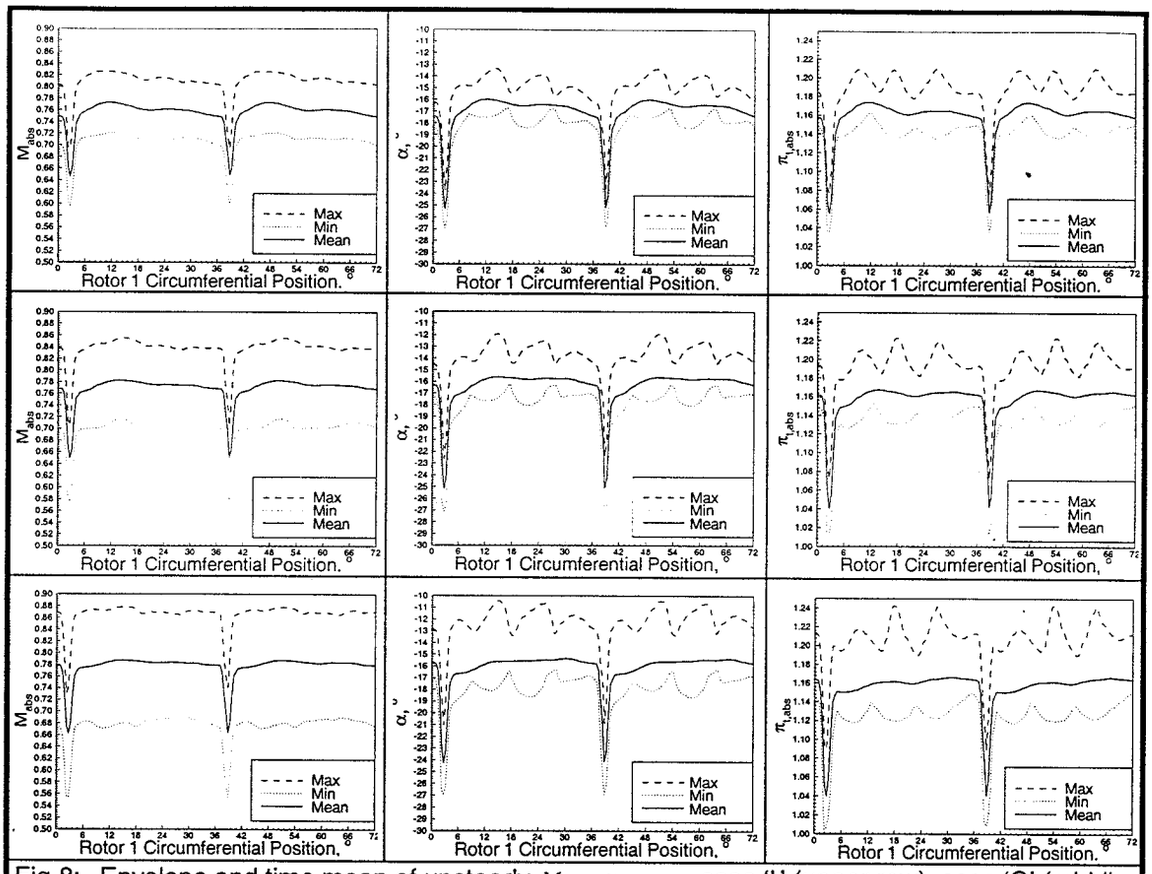

Fig.8: Envelope and time mean of unsteady M_{abs}, α, $p_{t,abs}$ case 'L' (upper row), case 'O' (middle row) and case 'S' (lower row) downstream of rotor 1.

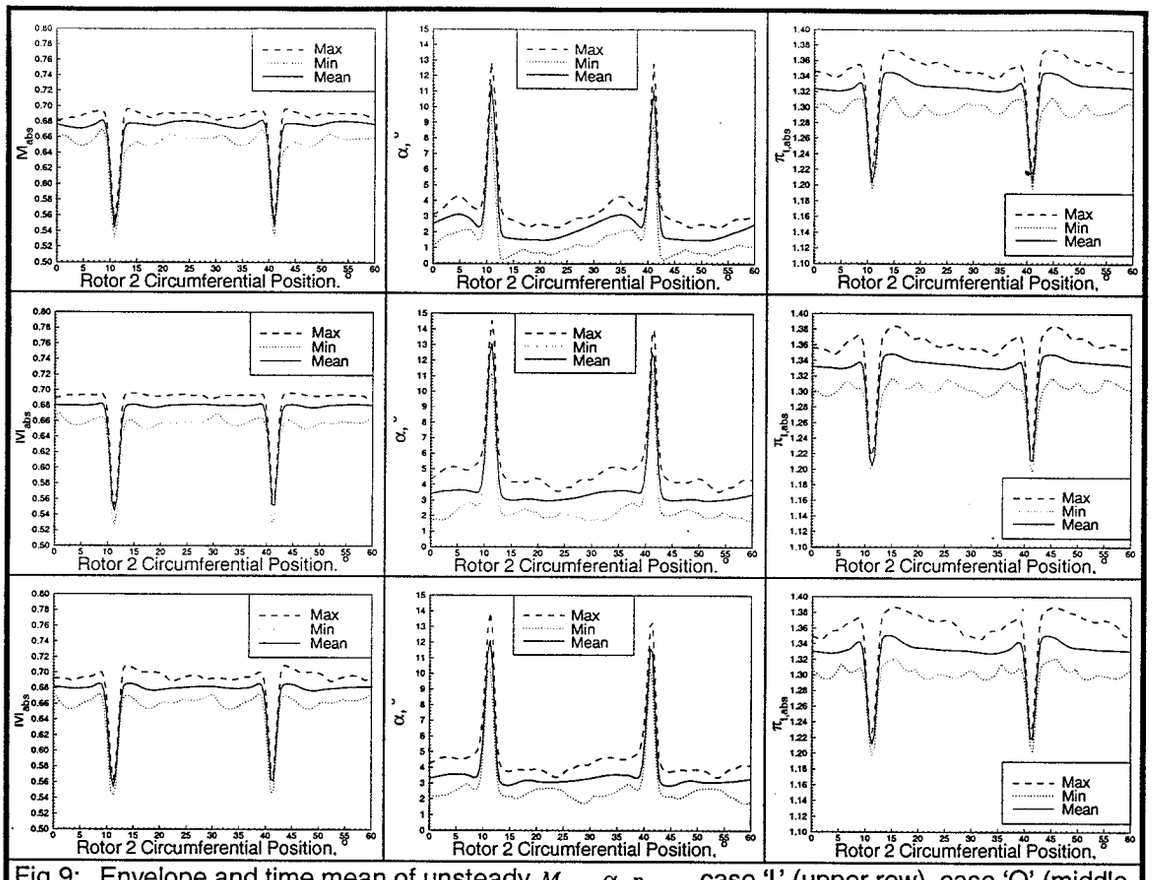

Fig.9: Envelope and time mean of unsteady M_{abs}, α, $p_{t,abs}$ case 'L' (upper row), case 'O' (middle row) and case 'S' (lower row) downstream of rotor 2.